Surface structure of silver nanoparticles as model for understanding oxidative release of silver ions

Bastiaan Molleman and Tjisse Hiemstra*

Supporting Information

(17 pages, 5 figures, 3 tables)

1 Literature data of Ag^+ release. Kinetics and equilibrium
2 Spheroidal nanoparticle morphologies
2.1 Cuboctahedra
2.2 Icosahedra
2.3 Surface calculation for icosahedra
3 Bond valence analyses
3.1 Calculating the bond valence
3.2 Varying the reference bond length
3.3 Soft bond valence
4 Silver compounds with a layered crystal structure
5 MO/DFT computation
5.1 Geometry optimization
5.2 Energy calculations
6 Collected literature data
7 References

*Corresponding author's email address: **tjisse.hiemstra@wur.nl**
Phone: +31 317 48 2342; Fax: +31 317 41 9000
Department of Soil quality, Wageningen University,
P.O. Box 47, 6700 AA Wageningen, The Netherlands

1 Ag^+ release literature data

Ag^+ release from silver nanoparticles (AgNPs) has been measured on several occasions in recent years. Figure S1 shows collected time dependent release data as could be distilled from published graphs. Note the quick initial release and the long-term stability of the concentrations that are eventually reached. Data by Sotiriou et al. (2012) distinguish themselves from the other datasets by the extremely short dissolution times (< 2 hours), this is possibly due to a different AgNP production method (flame spray pyrolysis and wet impregnation) which include a high temperature step under water-free conditions.

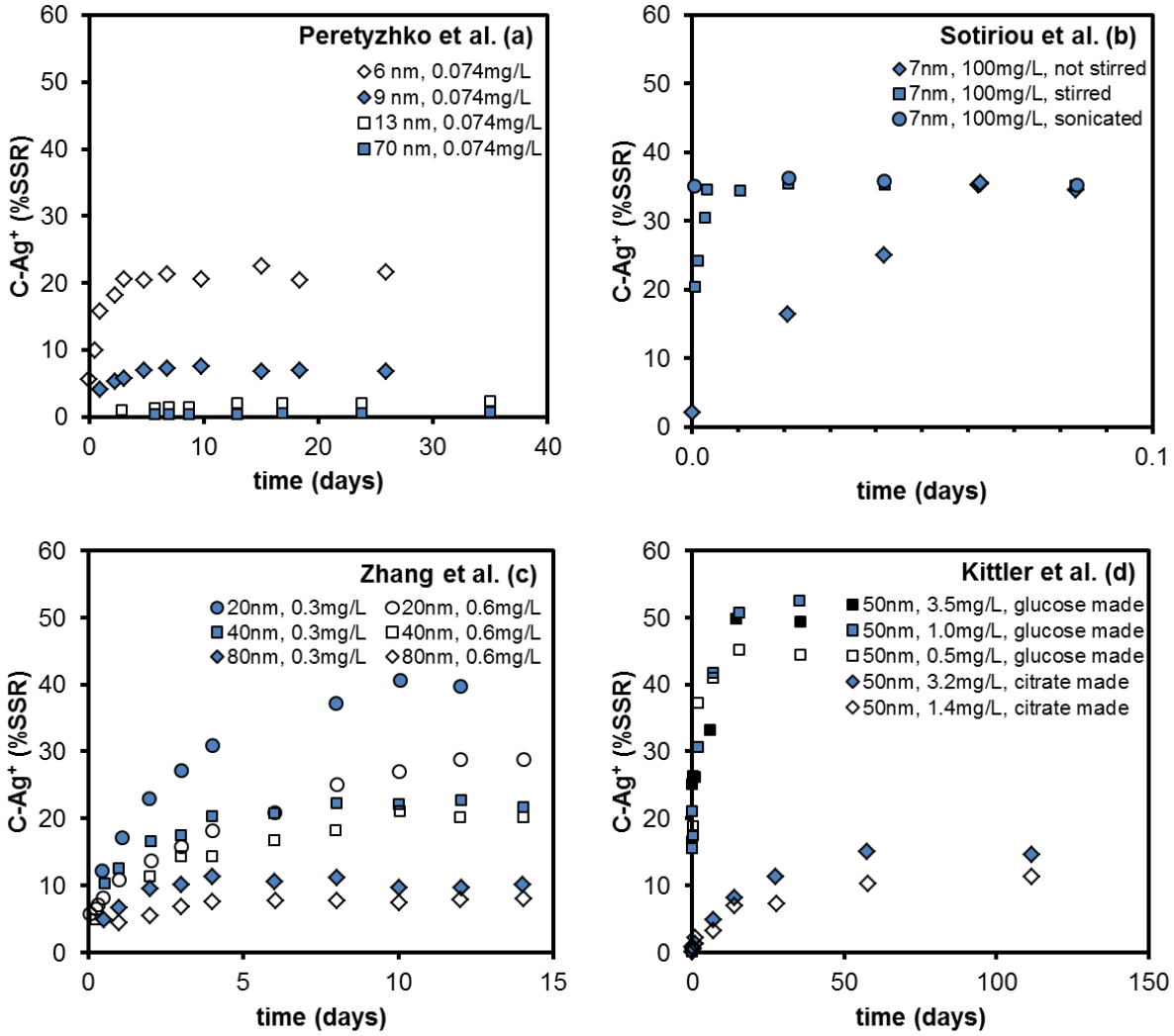

Figure S1: *Ag^+ release data of several AgNP dissolution experiments from recent literature. Experimental parameters (e.g. particle size, preparation method, capping agent, solid solution ratio) are highly variable between datasets.*

a) Ion release data from Peretyazhko et al. (2014), using four different particle sizes at a single SSR. AgNPs were reduced using $NaBH_4$ (6nm), citrate (70nm), or both (9 and 13nm, seeded with $NaBH_4$ and grown with citrate), and capped with thiolated PEG. Ag^+ concentrations are measured with an ion-selective electrode. In all figures Ag^+ release is expressed as a percentage of the SSR.

b) Ion release taken from Sotiriou et al. (2012), using flame-made AgNPs at a high SSR. Ag^+ concentrations are determined using ion selective electrode and ion meter.

c) Ion release taken from Zhang et al. (2011), citrate coated AgNPs of unknown production method (purchased) of different sizes were used at two different SSR. Ag^+ concentrations were determined by ultrafiltration and ICP-MS.

d) Ion release taken from Kittler et al. (2010), AgNPs were placed in dialysis bags, which were placed in a 100-fold excess of ultrapure water. Two types of particles were used, one was reduced by glucose and coated with PVP, the other had citrate as both the reductant and capping agent. Both particles had a size of 50 nm.

2 Spheroidal nanoparticle morphologies

2.1 Cuboctahedra

In the fcc crystal structure, near spherical, single crystals can be made which are called cuboctahedra (Figure S2a). These structures are bounded by (111) and (100) faces. How much these faces contribute to the total surface area depends on the ratio between the distances between opposing crystal faces. The (111) face tends to be dominant (75 ± 11%).

2.2 Icosahedra

Surface tension greatly contributes to the total free energy of a nanoparticle. This may lead to different morphologies than are expected based on the crystal structure of a substance. In metal nanoparticles this often leads five-fold twinning (Hofmeister, 2004), which may result in an icosahedral structure (Figure S2b). The outer surface has only (111) faces, minimizing surface tension; the internal crystal symmetry is only minimally distorted.

2.3 Surface calculations for icosahedra

A regular icosahedron consists of 20 triangular faces. The number of atoms in a single triangle is equal to

$$x_n = \frac{n^2 + n}{2}$$

where n is the number of atoms at the base of a triangle. As edge and corner atoms (shown in Figure S3) are shared between faces, the number of surface atoms is less than $20x$. We can calculate the effective number of atoms per triangle, x_{eff}, by subtracting the shared atoms from x. Corner atoms in the structure are shared between five faces, and edge atoms are shared

between two faces, as is shown in Figure S3, there are three corner atoms and $3(n-2)$ edge atoms in each triangle, leading to:

$$x_{\text{eff, } n} = x - 3\frac{(n-2)}{2} - 3\frac{4}{5}$$

The number of surface atoms is equal to $20x_{\text{eff, n}}$, number of total atoms may be calculated by taking the sum of the successive surface layers. With these equations one may find the relationship between, specific surface area and the effective diameter d_{eff}, taking for the diameter the distance between the middle of opposing ribs of the icosahedron, which is given by:

$$d_{\text{eff}} = 2r_{\text{eff}} \approx 2 \cdot 0.809 \cdot n \cdot d_{\text{Ag-Ag}}$$

where $d_{\text{Ag-Ag}}$ is the bond length between silver atoms in the metallic silver crystal lattice.

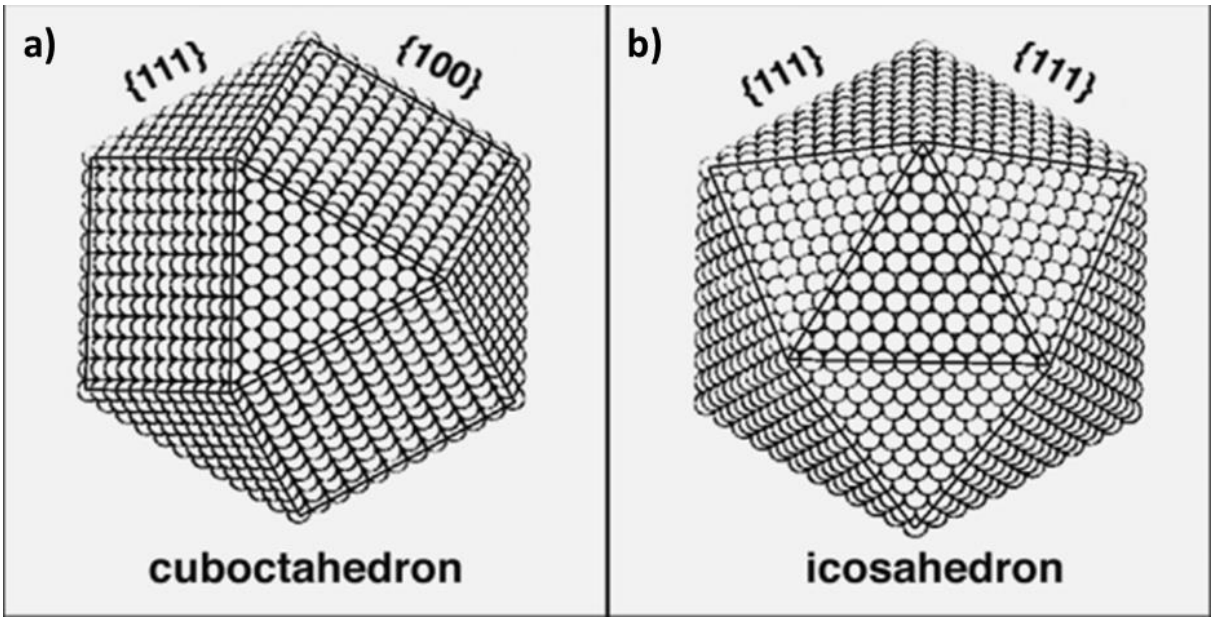

Figure S2: Two types of spheroidal nanoparticles which may occur in the fcc crystal lattice, taken from Hofmeister (2004).
a) a singly crystalline cuboctahedron having both the (111) and the (100) plane at the surface
b) a fivefold twinned icosahedron with exclusively (111) plane surfaces.

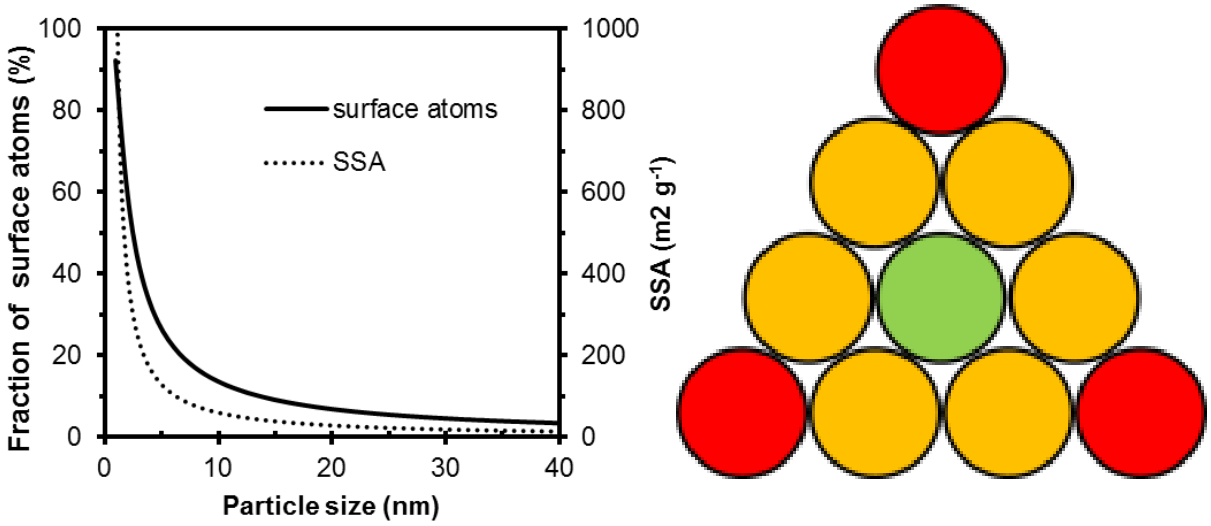

Figure S3: The relationship between particle diameter and specific surface area and percentage of surface atoms. Also shown is a triangular (111) face with base n=4, with corner atoms (shared between 5 faces) shown in red, and edge atoms (shared between two faces) shown in orange.

3 Bond valence analyses

An empirical relationship between bond length, *R*, and bond valence, ν, is found to exist in minerals of the same cation (Brown and Altermatt, 1985). We have studied the crystal structures of various silver oxides in order to analyze this relationship for this class of minerals.

3.1 Calculating the bond valence

Bond valences were calculated according to the empirical relationship between bond length, *R*, and bond valence, ν (Brown and Altermatt, 1985).

$$\nu = \mathrm{e}^{-(R-\mathrm{R_0})/\mathrm{B}} \quad (1)$$

where R_0 is the reference bond length (184.2 pm), which is cation specific, and B is a chosen constant (37 pm), which is traditionally kept constant for all compounds (Brown and Altermatt, 1985). From crystallographic data (see Table S1 for references) the coordination numbers bond lengths were extracted. In most crystal structures, more than one bond length can be found. Bond lengths were grouped together if differences were very small, otherwise they were treated separately. The coordination number refers to the number of bonds of the given bond length that were attached to the cation.

3.2 Varying the reference bond length

If the reference bond length, R_0, is kept constant at its reference value of 184.2 pm (Brown and Altermatt, 1985), the sum of the bond valences may be larger or smaller than the charge of the cation. Therefore, R_0 was varied by trial and error until the sum of the bond valences was equal to the charge of the cation. R_0 of a given element, may vary with oxidation state (Brown and Altermatt, 1985); therefore, in the case of AgO, or more correctly Ag(I)Ag(III)O_2, a different value was used to the two types of Ag found in its crystal structure.

3.3 Soft bond valence

It is known that the empirical bond valence-bond strength relationship cannot be solved for all crystal structures. In the case of Ag_2O_3, the optimization approach described above led to a sum of bond valences around the oxygen anion which was not equal to 2. This problem can be overcome by choosing a different value (29 pm) for the constant B. To keep things comparable, we have chosen to maintain the standard value for B (37 pm).

144 *Table S1: Overview of bond valences calculated by adjusting the reference bond strength, R_0,*
145 *so that the sum of the bond valences, ν, equals the charge of the silver cation, z_{Ag}. References*
146 *concern the crystallographic data from which bond lengths, R, and coordination numbers,*
147 *CN, were taken.*

148

	z_{Ag}	R_0	CN	R	ν	Reference
Ag_3O	+⅔	188.5	2	229.2	0.33	(Beesk et al., 1981)
Ag_2O	+1	180.5	2	206.1	0.50	(Wyckoff, 1922)
Ag^+(aq)	+1	187.9	2	232	0.30	(Persson and Nilsson, 2006)
			2	248	0.20	
AgO	+3	189.2	4	202.0	0.71	(Yvon et al., 1986)
			2	279.6	0.09	
	+1	182.8	2	216.7	0.40	
			2	267.8	0.10	
Ag_2O_3	+3	187.0	1	191.6	0.88	(Standke and Jansen, 1986)
			2	202.5	0.66	
			1	204.6	0.62	
			1	269.9	0.11	
			1	285.3	0.07	
Ag_2F	+½	180.4	3	246.7	0.17	(Ott and Seyfarth, 1928)
Ag_2NiO_2	+½	184.8	2	252.7	0.16	(Wedig et al., 2006)
			1	248.1	0.18	
$AgNiO_2$	1	186.6	2	212.2	0.50	(Shin et al., 1993)
$Ag_{13}OsO_6$	+⅓	179.2	2	245.5	0.17	(Ahlert et al., 2003)

149

4 Silver compounds with a layered crystal structure

Several silver compounds can be found with a layered structure. When silver is present in a bilayer, it may assume a subvalent oxidation state, as in Ag_2F, Ag_6O_2, and Ag_2NiO_2. When only a single layer of Ag is present, as in $AgNiO_2$, subvalence is not observed. The crystal structures of Ag_2F, Ag_6O_2, Ag_2NiO_2, and $AgNiO_2$ are given in Figure S4.

The view presented in Figure S4 focusses on the presence of silver bilayers in the structure and may therefore appear at odds with the bond valence analyses of Ag_6O_2 and Ag_2F in the main text, which focusses on the octahedra. To clarify this matter, we point out that the Ag-O-Ag and Ag-F-Ag slabs, in which said octahedra can be identified, form Ag-bilayers when stacked together.

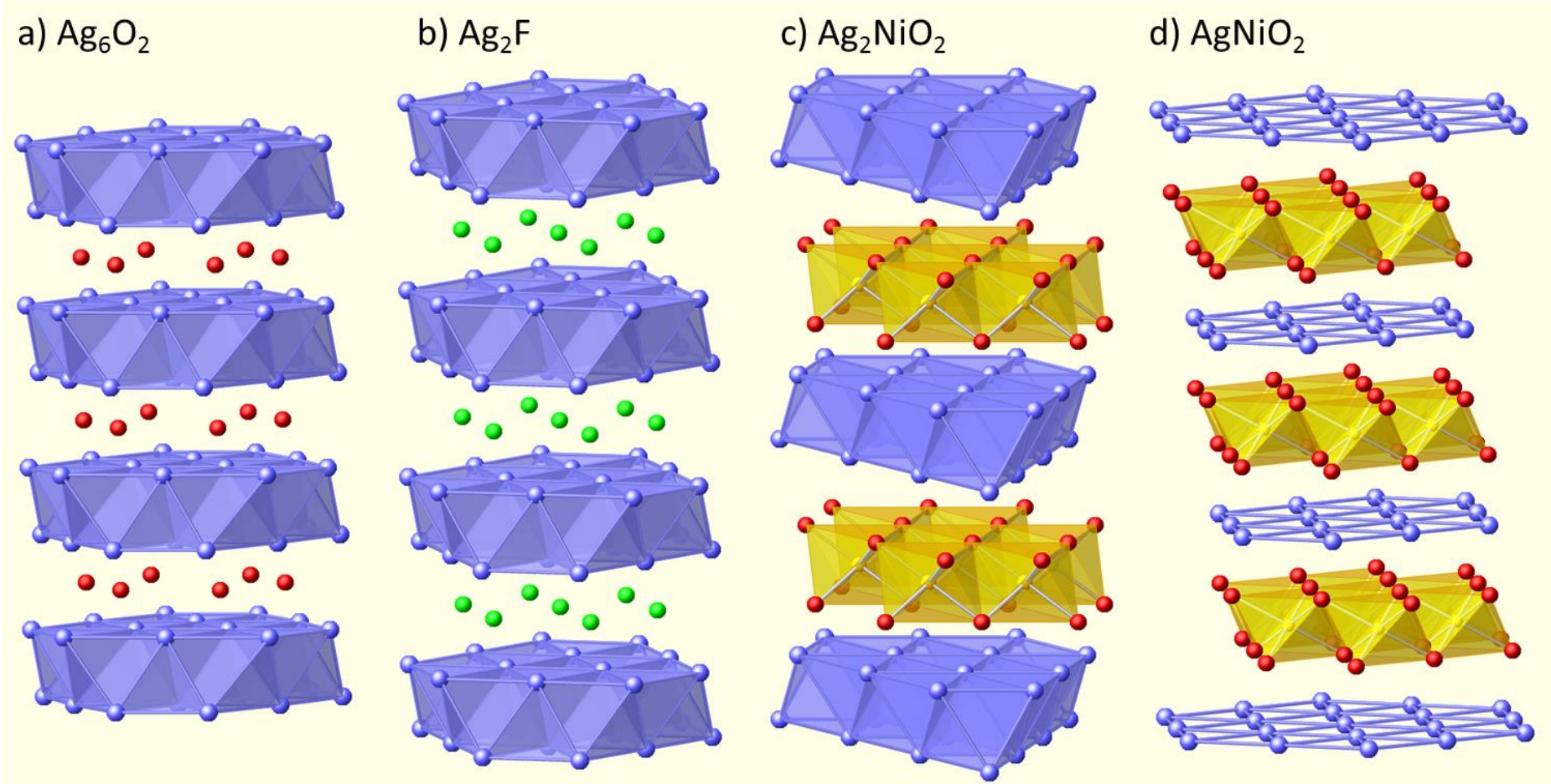

Figure S4: Subvalent and classical layered silver compounds. Silver ions are shown in blue, oxygen in red, fluoride in green and nickel is shown in yellow. Polyhedral plains are drawn to emphasize subvalent silver bilayers and nickel octahedra as structural units. Figures were made using CrystalMaker®, inspired by the Max Planck institute for solid state research.

5 MO/DFT computation

The quantum mechanical optimization program Spartan 06 was used to evaluate the energies and molecular configurations of Ag_{13} clusters with various states of subvalency.

5.1 Geometrical optimization

As is discussed in the main text, the metallic Ag13-cluster has a regular icosahedral shape, which becomes slightly distorted if 4 -OH groups are placed on its surface. If the structure is further oxidized, and 4 -O groups are placed on the surface, the icosahedral structure becomes severely distorted, as is shown below (Figure S5).

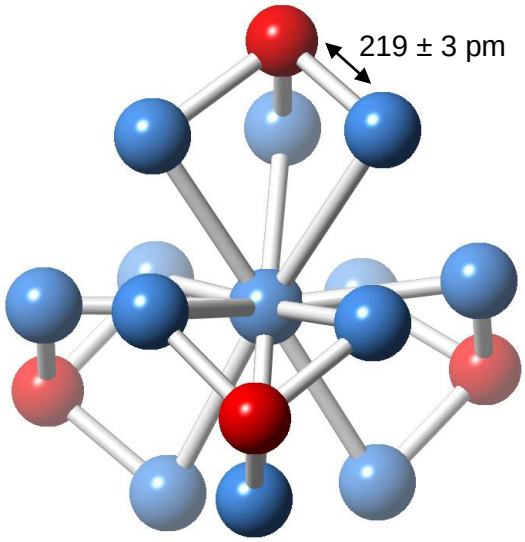

Figure S5: The optimized structures of a $Ag_{13}O_4$ cluster. Distortion of the initial Ag_{13}-cluster is most obvious in the four forward silver atoms in a nearly square formation: in the optimized Ag_{13}-cluster, these form two triangular planes.

5.2 Energy calculations

The final structure is optimized by finding the molecular configuration with the lowest possible energy contents. Quantum mechanical calculations are analytically solved an may not provide perfectly accurate anwers, but they give us a good first impression of chemical stabillity of different Ag-clusters.The complete enthalpy (H) of a structure is made up of the complete elecronic energy (E_e), the zero point energy of the nuclei (Z_0), the vibrational enthalpy (H_v), enthalpy due to rigid body translation and rotation (H_t and H_r, respectively), and a pressure term from the ideal gas law equation ($pV = RT$). By correcting the complete enthalpy for vibrational entropy (S_v) and entropy of rigid body translation and rotation (S_t and S_r, respectively), the Gibb's free energy (G) of a structure is obtained. Results of the geometrical optimizations can be found in Table S2.

Using the obtained Gibb's free energies, the Gibb's free energy change of a reaction, ΔG_r, can be found by subtracting the combined Gibb's free energy of the reactants from the combined Gibb's free energy of the reaction products. As an example, we will calculate the Gibb's free energy change of the transformation of $Ag_{13}O_4$ into $Ag_{13}(OH)_4$:

$$Ag_{13}O_4 + 2H_2O \leftrightarrow Ag_{13}(OH)_4 + O_2 \quad (2)$$

The reactions has a highly negative Gibb's free energy change:

$$\Delta G_r = G_{Ag_{13}(OH)_4} + G_{O_2} - 2G_{H_2O} - G_{Ag_{13}O_4} = -176\ \mathrm{kJ/mol} \quad (3)$$

showing that, at atmospheric oxygen pressures and in the presence of water, $Ag_{13}O_4$ is highly unstable and will almost certainly be transformed in to $Ag_{13}(OH)_4$ under release of oxygen gas.

Table S2: calculated energy terms for the optimized structures. Energy terms are given in kJ/mol for ambient temperature and pressure of 298.15 °K and 1 bar, respectively.

	Ag_{13}	$Ag_{13}O_4$	$Ag_{13}(OH)_4$	H_2	O_2	H_2O
E_e	-4977304.6090	-5766555.5950	-5773447.0254	-3060.3891	-394326.3640	-200507.2654
Z_0	9.5152	24.2536	153.4747	26.5347	9.9001	55.8086
H_v	45.7091	40.0642	73.2393	0	0.0067	0.0054
H_t	3.7184	3.7184	3.7184	3.7184	3.7184	3.7184
H_r	3.7184	3.7184	3.7184	2.4789	2.4789	3.7184
pV	2.4789	2.4789	2.4789	2.4789	2.4789	2.4789
S_v	119.5875	94.3738	168.5380	0	0.0076	0.0061
S_t	59.3323	59.4996	59.5099	35.0289	45.3084	43.1723
S_r	47.2934	47.9451	47.9927	3.8162	14.8042	13.1094
H	-4977239.4690	-5766481.3615	-5773210.3957	-3025.1782	-394307.7810	-200441.5357
G	-4977465.6822	-5766683.1800	-5773486.4364	-3064.0233	-394367.9012	-200497.8236

6 Collected literature data

We have collected data from literature references which have performed AgNP dissolution experiments and which have measured Ag^+ concentration at *equilibrium*. We have carefully documented all available information on particles size, standard deviation, synthesis, capping agents and other relevant steps taken during sample preparation. Silver release data have been converted into a loading parameter by expressing the final Ag^+ concentrations per total AgNP surface area, according to:

$$\Gamma = \frac{[Ag^+]}{SA} = \frac{[Ag^+]}{SSR \cdot A} \quad (2)$$

where Γ is the surface loading (in mol/m^2), $[Ag^+]$ is the ionic silver concentration (in mol/L), *SA* is the total AgNP surface area (in m^2/L), *SSR* is the solid solution ratio (i.e., the initial AgNP concentration in g/L), *A* is the AgNP specific surface area (in m^2/g). Using

$$A = \frac{6}{d \cdot \rho_{Ag}} \quad (3)$$

where *d* is the AgNP diameter (in m) and ρ_{Ag} is the mass density of silver (in g/m^3), equation 2 can be rewritten to

$$\Gamma = \frac{[Ag^+] \cdot d \cdot \rho_{Ag}}{6 \cdot SSR} \quad (4)$$

Moreover, an average loading is given for the combined data points of each reference. Data and references can be found in Table S3.

Table S3: Overview of AgNPs and the reported silver release (Γ) expressed per unit surface area, as well as the mean release ($\bar{\Gamma}$) expressed in fractions of monolayers, where 1 monolayer is equal to the 2-dimensional silver density in the (111) face of silver (i.e. 23μmol/m^2)

Authors	Synthesis	Pretreatment	Reductant	Capping agent	Size (nm)	Γ (μmol m^{-2})	$\bar{\Gamma}$ (ML)
(Peretyazhko et al., 2014)	Wet synthesis by reduction	washed	$NaBH_4$*	PEG-SH	6.2 ± 1.6	20	0.3
	Wet synthesis by reduction	washed	$NaBH_4$*	PEG-SH	9.2 ± 3	11	
	Wet synthesis by reduction	washed	$NaBH_4$*	PEG-SH	12.9 ± 3.5	5	
	Wet synthesis by reduction	washed	Citrate	PEG-SH	70.5± 12	3	
(Ma et al., 2011)	Wet synthesis by reduction	washed	$NaBH_4$	GA	5.5 ± 1.7	43	1.0
	Wet synthesis by reduction	washed	Citrate	GA	22.8 ± 6	20	
	Wet synthesis by reduction	washed	$NaBH_4$	PVP	4.7 ± 1.6	46	
	Wet synthesis by reduction	washed	$NaBH_4$	PVP	8.4 ± 2.3	19	
	Wet synthesis by reduction	washed	Ethylene Glycol	PVP	26.3 ± 6.9	24	
	Wet synthesis by reduction	washed	Ethylene Glycol	PVP	38.2 ± 9.9	24	
	Commercial	washed	Not reported	None	50 ± 15	8	
	Commercial	washed	Not reported	PVP	76.6 ± 21	12	
(Sotiriou et al., 2012)	Flame spray pyrolysis	washed	-	none	4.0 ± 2.0	2	0.1
	Flame spray pyrolysis	washed	-	none	4.3 ± 3.2	2	
	Flame spray pyrolysis	washed	-	none	6.1 ± 3.1	3	
	Flame spray pyrolysis	washed	-	none	6.7 ± 4.1	3	
	Flame spray pyrolysis	washed	-	none	8.2 ± 3.4	5	
	Flame spray pyrolysis	washed	-	none	8.9 ± 3.5	4	
	Impregnation and annealed	none	-	none	4.6 ± 3.2	2	
(Sotiriou et al., 2012)	Flame spray pyrolysis only	none	-	none	4.0 ± 2.0	42	1.7
	Flame spray pyrolysis only	none	-	none	4.3 ± 3.2	44	
	Flame spray pyrolysis only	none	-	none	6.1 ± 3.1	44	
	Flame spray pyrolysis only	none	-	none	6.7 ± 4.1	38	
	Flame spray pyrolysis only	none	-	none	8.2 ± 3.4	34	
	Flame spray pyrolysis only	none	-	none	8.9 ± 3.5	29	
	Impregnation and annealed	none	-	none	4.6 ± 3.2	43	
(Zhang et al., 2011)	Commercial product	none	Not reported	Citrate	20 ± 0.5	123	4.9
	Commercial product	none	Not reported	Citrate	40 ± 0.6	130	
	Commercial product	none	Not reported	Citrate	80 ± 0.7	124	
(Kittler et al., 2010)	Wet synthesis by reduction	none	Citrate	Citrate	50 ± 20	98	4.3
	Wet synthesis by reduction	none	Glucose	PVP	50 ± 20	364	16

* Particles were produced from $NaBH_4$ reduced particles, and grown in a hot citrate medium

Washing step was included before use in contrast to the initial samples given in the series of rows below

7 References

Ahlert, S., Klein, W., Jepsen, O., Gunnarsson, O., Andersen, O.K. and Jansen, M. (2003) $Ag_{13}OsO_6$: A Silver Oxide with Interconnected Icosahedral Ag_{13}^{4+} Clusters and Dispersed $[OsO_6]^{4-}$ Octahedra. Angewandte Chemie International Edition 42, 4321.

Beesk, W., Jones, P.G., Rumpel, H., Schwarzmann, E. and Sheldrick, G.M. (1981) X-Ray Crystal Structure of Ag_6O_2. Journal of the Chemical Society, Chemical Communications, 664-665.

Brown, I.D. and Altermatt, D. (1985) Bond-valence Parameters Obtained from a Systematic Analysis of the Inorganic Crystal Structure Database. Acta Crystallographica Section B 41, 244-247.

Hofmeister, H. (2004) Fivefold Twinned Nanoparticles. Encyclopedia of Nanoscience and Nanotechnology 3, 431.

Kittler, S., Greulich, C., Diendorf, J., Koller, M. and Epple, M. (2010) Toxicity of Silver Nanoparticles Increases during Storage Because of Slow Dissolution under Release of Silver Ions. Chemistry of Materials 22, 4548-4554.

Ma, R., Levard, C.m., Marinakos, S.M., Cheng, Y., Liu, J., Michel, F.M., Brown, G.E., Jr. and Lowry, G.V. (2011) Size-Controlled Dissolution of Organic-Coated Silver Nanoparticles. Environmental Science & Technology 46, 752-759.

Ott, H. and Seyfarth, H. (1928) XXVIII. Die Struktur des Silbersubfluorids Ag_2F. Zeitschrift für Kristallographie - Crystalline Materials 67, 430-433.

Peretyazhko, T.S., Zhang, Q. and Colvin, V.L. (2014) Size-Controlled Dissolution of Silver Nanoparticles at Neutral and Acidic pH Conditions: Kinetics and Size Changes. Environmental Science & Technology 48, 11954-11961.

Persson, I. and Nilsson, K.B. (2006) Coordination Chemistry of the Solvated Silver(I) Ion in the Oxygen Donor Solvents Water, Dimethyl Sulfoxide, and N,N‘-Dimethylpropyleneurea. Inorganic Chemistry 45, 7428-7434.

Shin, Y.J., Doumerc, J.P., Dordor, P., Delmas, C., Pouchard, M. and Hagenmuller, P. (1993) Influence of the Preparation Method and Doping on the Magnetic and Electrical Properties of $AgNiO_2$. Journal of Solid State Chemistry 107, 303-313.

Sotiriou, G.A., Meyer, A., Knijnenburg, J.T.N., Panke, S. and Pratsinis, S.E. (2012) Quantifying the Origin of Released Ag^+ Ions from Nanosilver. Langmuir 28, 15929-15936.

Standke, B. and Jansen, M. (1986) Darstellung und Kristallstruktur von Ag_2O_3. Zeitschrift für anorganische und allgemeine Chemie 535, 39-46.

Wedig, U., Adler, P., Nuss, J., Modrow, H. and Jansen, M. (2006) Studies on the electronic structure of Ag_2NiO_2, an intercalated delafossite containing subvalent silver. Solid State Sciences 8, 753-763.

Wyckoff, R.W.G. (1922) The crystal structure of silver oxide (Ag 2 O). American Journal of Science 5, 184.

Yvon, K., Bezinge, A., Tissot, P. and Fischer, P. (1986) Structure and magnetic properties of tetragonal silver (I, III) oxide, AgO. Journal of Solid State Chemistry 65, 225-230.

Zhang, W., Yao, Y., Sullivan, N. and Chen, Y.S. (2011) Modeling the Primary Size Effects of Citrate-Coated Silver Nanoparticles on Their Ion Release Kinetics. Environmental Science & Technology 45, 4422-4428.